Photothermal studies of single molecules and gold nanoparticles : vapor nanobubbles and conjugated polymers

Hou, L.

4

Time-resolved study of vapor nanobubbles in water around a continuously laser-heated gold nanoparticle

Abstract– *We apply picosecond pump-probe spectroscopy to investigate the formation of vapor nanobubbles around a continuously heated gold nanoparticle in water. The aim of this experiment is to simulate the explosions observed under continuous heating, but by triggering the explosions by a short pump pulse. We obtain time traces of vapor bubbles with picosecond time resolution, apparently synchronized with the pump pulse. We observe a characteristic interference feature in the time trace and a strong modification of the signature of acoustic vibrations of the gold nanoparticle.*

4.1. Introduction

Studies of vapor nanobubbles have attracted more attention in recent years not only because their transient nature and thermodynamics have not been fully understood [22], but also because nanobubbles could be useful in applications such as photothermal therapy [6, 9, 89], drug delivery [7], solar steam generation [35], as contrast agents to enhance photo-acoustic couplings [10] and for chemical reactions [11, 90]. One way of generating vapor nanobubbles is to heat a liquid locally using a laser beam in the presence of nanoabsorbers such as gold nanoparticles to enhance the absorption efficiency [91]. Due to the fast excitation and relaxation of electrons and phonons and to the high thermal conductivity of the metal, a homogeneous temperature distribution is established in the gold nanoparticle after a few picoseconds. Subsequent heat transfer into the surrounding liquid in a few hundred picoseconds can initiate boiling of the liquid in the vicinity of the gold nanoparticle. The dynamics of the ensuing vapor bubble has not been characterized at the single bubble level on the sub-nanosecond timescale. Liquid superheating has been observed in many rapid heating processes [26, 28, 66] and is often accompanied by explosive boiling. Experiments with pulsed or continuous lasers have been extensively carried out to uncover the physical and thermal properties of vapor nanobubbles [8, 36, 92]. For example, vapor nanobubbles around gold nanoparticles have been studied using photothermal microscopy [30], bright-field optical scattering [73, 93], and dark-field spectroscopy [39] with time resolutions down to nanoseconds. Time-resolved pump-probe spectroscopy with picosecond lasers has been applied to study the spectral changes due to vapor bubbles around gold particles as a function of time delay [74], but the measurements were done in solution with several particles in the excitation volume. Pump-probe experiments with pulsed X-rays as the probe beam were performed to resolve the dynamics of vapor bubbles [26, 32, 94], providing the high sensitivity of X-ray scattering and diffraction to the structural changes of gold nanoparticles and of the surrounding water molecules, but the time resolution was limited to 100 ps because of the width of the electron beam, and the measurements are still done at the ensemble level, with several particles in the excitation focus.

Due to the fast dynamics and transient nature of vapor nanobubbles, it is quite challenging to investigate these at the single-nanoparticle level without averaging the contributions from nearby particles. The transient behavior of vapor nanobubbles also requires a high time resolution of detection in the sub-nanosecond timescale. Only then can the evolution of vapor nanobubbles during the initial stages after excitation be better resolved. In this chapter,

we combine continuous-wave (CW) heating with time-resolved pump-probe spectroscopy to study the transient behavior of vapor nanobubbles in water around a single gold nanosphere. The CW heating beam brings the temperature of the gold nanoparticle close to the boiling threshold of water, and the pump pulse drives the system out of equilibrium and triggers the dynamics of the vapor nanobubble on the picosecond timescale. We record transient traces of vapor nanobubbles upon femtosecond excitation under high CW heating and show that we can obtain picosecond time resolution in a time window of one nanosecond.

4.2. Experimental details

Time-resolved pump-probe measurements of vapor nanobubbles were done on a home-built horizontal microscope. A scheme of the optical setup is shown in Fig.4.1. A femtosecond pulse (about 300 fs) with central wavelength 785 nm from a Ti: sapphire laser (76 MHz repetition rate) is used as the pump source. The probe pulse is the synchronized frequency-doubled output of an optical parametric oscillator (OPO, tunable wavelength from 590 nm to 640 nm) [95]. This OPO is pumped by the above Ti: sapphire laser. A continuous wave (CW) laser at 532 nm is spatially overlapped with the two pulsed beams. The three beams are sent into the microscope and focused on the sample with an oil-immersion objective (Olympus, NA=1.4). The intensity of the pump beam is modulated with an acousto-optical modulator at 450 kHz. The probe wavelength is chosen around 597 nm where the surface plasmon resonance (SPR) of single gold nanospheres is most sensitive to the changes of the refractive index of the surrounding medium. The transmitted light is collected by a second objective with a numerical aperture of 0.75, and is focused on a photodiode detector (FEMTO). A set of optical filters were placed in front of the detector in order to remove both the continuous and pump beams. Time delays between pump and probe pulses are controlled with a linear mechanical stage, which can move continuously and alter the propagation delay of the pump pulse. The signal of the photodiode is demodulated at the modulation frequency of the pump by a lock-in amplifier to extract the small change ΔT in the intensity of the transmitted probe beam. This ΔT was recorded as a function of time delay by a digital-analog converter (ADwin gold) and home-built Labview software. The alignment was optimized by maximizing the photothermal signal of a single gold nanosphere in water.

Gold nanospheres are purchased from BBI (British Biocell International). Their average diameter is about 50 nm. The cover slides are rinsed in acetone, ethanol and pure water separately and are cleaned in an ozone cleaner to re-

move all the possible impurities and organic contaminants. Gold nanoparticles are then spin-coated on clean cover slides. Concentration and spin-coating parameters are adjusted so that gold nanoparticles are well isolated from each other on the cover glass. Then the cover slide coated with gold nanoparticles is attached to a home-built flow cell made of Polydimethylsiloxane (PDMS). Milli-Q water was used in all the experiments. Positions of single gold nanoparticles are determined with the pump-probe microscope and time delay set to zero.

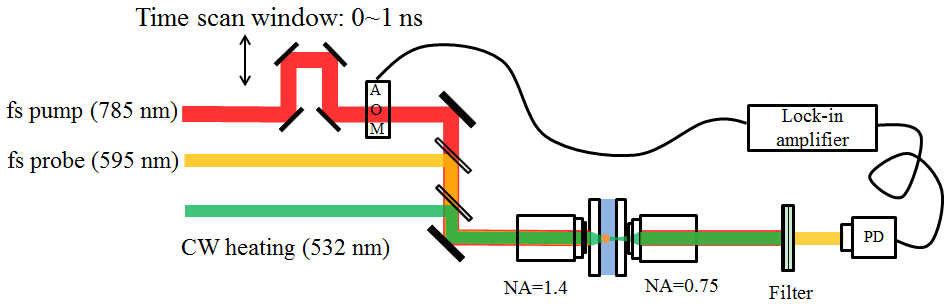

Figure 4.1: Scheme of the experimental setup for the time-resolved study of vapor nanobubbles. PD: photodiode; AOM: acousto-optic modulator.

4.3. Cooling kinetics and acoustic vibrations of a gold nanoparticle

Upon laser excitation, the following processes take place in successive steps. First, the SPR is excited by the pump pulse as a collective oscillation of the metal's conduction electrons. Subsequently, after some ten femtoseconds, the SPR relaxes through relaxation of the electrons, leading to a hot electron gas. Due to the small heat capacity of the Fermi gas, the electron temperature rises by thousands of Kelvins. Electron-electron scattering then redistributes the absorbed energy over the entire electron distribution, forming a hot electron gas on the timescale of hundreds of femtoseconds. On a longer timescale of a few picoseconds, the electrons transfer their excess energy to the gold lattice. Because of its relatively large thermal capacity, the gold lattice heats up to lower temperatures, typically some tens of Kelvin in one to a few picoseconds, as resolved by transient pump-probe spectroscopy [46]. On still longer times, which depend on the interfacial resistance and on the conductivity of the medium, the hot particle thermalizes with its environment. This time is typically a few hundred picoseconds in the case of our particles [48]. Eventually, the particle returns to the initial unperturbed state.

We adopt the modified "two-temperature model" (TTM) to describe the energy deposition into the electron system, its subsequent relaxation to the metal

lattice and the surrounding medium, and the temperature evolution in these subsystems is written as [96]:

$$\begin{cases} C_e(T_e)\dfrac{\partial T_e(t)}{\partial t} = -G(T_e - T_l) + S(t) \\ C_l(T_l)\dfrac{\partial T_l(t)}{\partial t} = G(T_e - T_l) - F \\ C_m\dfrac{\partial T_m(t)}{\partial t} = \nabla \cdot [\kappa_m \nabla T_m(r,t)] + F \end{cases} \tag{4.1}$$

where C_e, C_l, and C_m are the heat capacities of electrons, lattice, and surrounding medium (water in our case), respectively. T_e, T_l, T_m are the temperatures of electrons, lattice, and water medium; G is an electron-phonon coupling coefficient and is taken from ref.[97]; κ_m is the thermal conductivity of liquid water; $S(t)$ is the laser excitation function, and is adopted as the same function as ref.[98], assuming a 300 fs pulse width with a Gaussian intensity profile; F is the term that governs the heat exchange at the particle-liquid interface, and can be expressed as $F \approx \frac{g}{R}[T_l - T_m(r = R)]$ [98] (g is the interface thermal conductance, experimentally determined to be 105 MW m^{-2}K^{-1} for 35 nm gold in water [99], R is the particle radius. This resistance corresponds to a water thickness of 6.5 nm). The first and second lines describe the electron-phonon coupling in the gold nanoparticle. The third line is the equation of heat diffusion in the surrounding medium.

We numerically solve the above equations to see how the temperatures of these subsystems evolve with time. The result is shown in Fig.4.2. It confirms that electron-phonon coupling in the particle and phonon-phonon coupling between particle and liquid take place in subsequent time steps. The temperature of electrons shoots up by thousands of Kelvin after the excitation because of the small heat capacity of electrons. Then the electron and lattice equilibrate in a few picoseconds, while the heat exchange between hot lattice and surrounding water takes place subsequently within 100 ps because of the low water conductivity and the interfacial thermal resistance between gold nanoparticle and liquid. The temperature of the nearby liquid starts to rise around 100 ps after the excitation, and thermal energy will become available to the surrounding liquid for possible liquid ebullition and bubble formation if enough energy is injected. Therefore, in the present case of heating by the pump pulse only, the liquid cannot boil before it has received the pump energy through conduction. In our experiments described later, a major part or whole of the energy required for boiling is coming from the continuous heating beam, prior to triggering by the pump pulse.

Another interesting phenomenon accompanying lattice relaxation is the coherent vibrational motion of the gold lattice, which is excited by two main

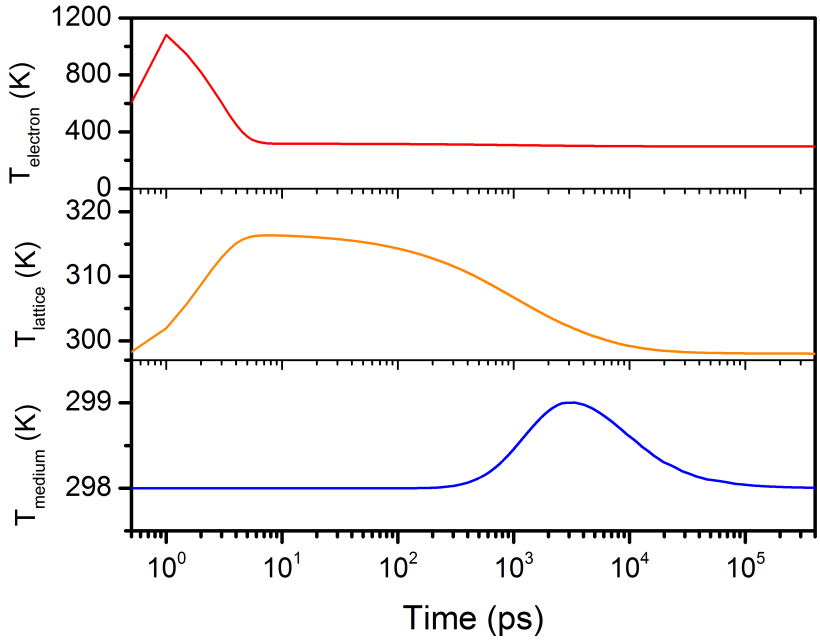

Figure 4.2: Calculated temperature evolution of the electrons (red, top), the lattice (orange, middle) and the surrounding water layer 1 nm away from the particle surface (blue, bottom) as a function of time upon femtosecond laser excitation. The fluence of the 785 nm 300 fs pulse is 5.3 mJ/cm^2. The initial temperature is set to 298 K.

mechanisms. First, the fast increase in the electronic temperature upon excitation leads to a sudden increase in Fermi pressure, which pushes the surface of the particle outward, giving an initial velocity to the expansion movement after cool down of the electrons. Second, the heating of the gold lattice consecutive to the electronic cool down leads to lattice expansion and to a new equilibrium radius. Both processes are faster than the typical period of the particle's breathing mode (about 17 ps for our 50 nm spheres). They both contribute to initial conditions different from equilibrium giving rise to the breathing oscillations of the particle.

The problem of the vibration motion of an elastic sphere has been theoretically solved by Lamb [100]. Two integers, the harmonic order n and angular momentum number l, describe the vibrational mode (n, l). For the spherical gold nanoparticles in our experiments, only the radially symmetric fundamental breathing mode (n, l)=(0, 0) will be excited. Lamb's theory may be complemented to find the vibrational frequency and the damping time of the breathing mode of an elastic gold sphere in an elastic medium according to the complex frequency model [101, 102]. These quantities are determined by the following

relations:

$$\omega_n + i\chi_n = \frac{\xi_n c_l^{(s)}}{R}, \tag{4.2}$$

$$\omega_n = Re(\xi_n)\frac{c_l^{(s)}}{R}, \qquad \chi_n = Im(\xi_n)\frac{c_l^{(s)}}{R}, \tag{4.3}$$

where ω_n is the vibration frequency; χ_n is the damping rate; R is the particle radius; $c_l^{(s)}$ is the longitudinal speed of sound in bulk gold. The complex eigenvalue ξ_n is determined by solving the following equation:

$$\xi cot\xi = 1 - (\frac{\xi^2}{\eta})\frac{1 + i\frac{\xi}{\alpha}}{\xi^2 - 4\alpha^2\zeta^2(1 - \frac{1}{\eta\beta^2})(1 + i\frac{\xi}{\alpha})}, \tag{4.4}$$

$$\alpha = c_l^{(m)}/c_l^{(s)}, \beta = c_t^{(m)}/c_t^{(s)}, \zeta = c_t^{(m)}/c_l^{(m)}, \eta = \rho^{(m)}/\rho^{(s)}, \tag{4.5}$$

where $c_{l,t}^{(m),(s)}$ are the longitudinal (l) and tranverse (t) sound velocity of matrix (m) and particle (s), $\rho^{(m),(s)}$ are the densities of water and gold.

Since the relaxation of excited electrons, lattice and nearby liquid take place in subsequent steps, we will look separately into the cooling kinetics of the gold nanoparticle, with and without a vapor nanobubble, depending on the heating power used. Note that the heating power we refer to is that of the continuous heating beam at 532 nm. The fluences of pump and probe pulses are low and kept constant during all measurements on the same particle. Control experiments show that, for the pump fluences we used, it was not possible to generate vapor bubbles without CW heating.

4.4. Results and discussion

4.4.1. Cooling kinetics of gold nanoparticle under variable CW heating power

In Fig.4.3, we show a typical pump-probe trace, measured without CW heating, of a 50 nm gold sphere immobilized on glass and immersed in pure water. The fluences of pump and probe pulses are low, and the initial temperature rise of the gold particle due to pump and probe pulsed heating are estimated according to the following equation [95]:

$$\Delta\ T|_{t=0} = \frac{\sigma_{abs} E_{pulse}}{A C_p V_p} \tag{4.6}$$

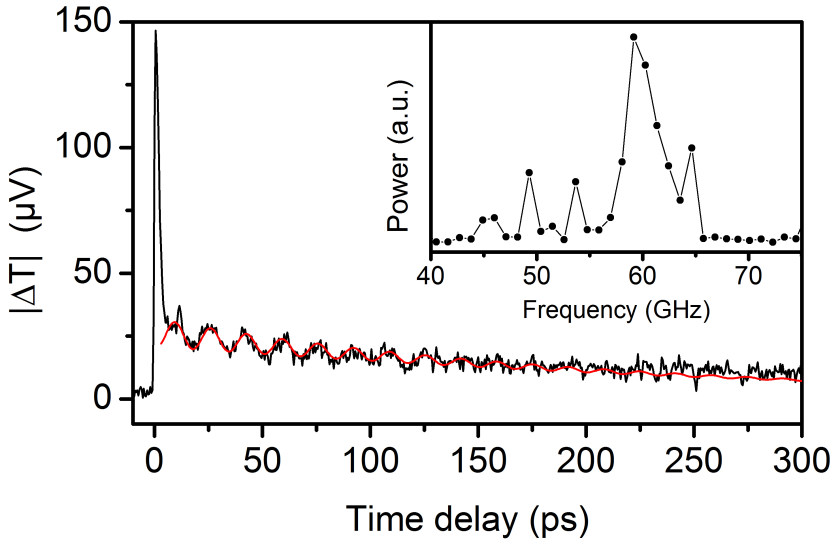

Figure 4.3: Time-resolved pump-probe trace of a 50 nm gold sphere immobilized on glass in water. There is no CW heating in this measurement. The red curve is a fitted curve showing the acoustic vibration of the single gold nanoparticle (with fitted parameters $\tau_1 = 283.3$ ps, $\tau_2 = 107.4$ ps, $A_1 = 26.5$ μV, $A_2 = 5.6$ μV, $T_{br} = 16.7$ ps, $\varphi = 2.7$ rad). The absolute value of the transmission change $|\Delta T|$ in the plot is the amplitude of the lock-in output. Insert: the power spectrum of the oscillatory part of the trace. The pump pulse energy at 785 nm with linear polarization is 26 pJ per pulse (average power is about 2 mW without transmission correction. The fluence is about 7.1 mJ/cm^2, assuming a diffraction-limited focal spot); the probe pulse energy at 597 nm is about 0.26 pJ (average power is 20 μW, fluence is about 0.1 mJ/cm^2). The integration time is 30 ms. All the powers and fluences mentioned in this chapter are measured before the objective.

where σ_{abs} is the absorption cross section of the gold particle, calculated from Mie theory, E_{pulse} is the energy of the incident pulse, A is the focus area assumed to have a diffraction-limited size; the absorbed energy E_{abs} is equal to $\sigma_{abs} E_{pulse}/A$; C_p and V_p are the specific heat capacity and the volume of the 50 nm diameter gold particle ($C_p = 24.9 \times 10^5$ J K^{-1}m^{-3}). The calculated temperature rises are shown in table 4.1. As mentioned earlier, three features, rep-

Table 4.1: Peak temperature rises of a gold nanoparticle generated by pump and probe lasers estimated from pulse fluences.

	σ_{abs}(nm^2)	E_{pulse}(pJ)	E_{abs}(fJ)	ΔT_p(K)
Pump at 785nm	65	26	4.6	28
Probe at 595nm	1470	0.26	1.8	11

resenting the relaxations of electrons, lattice and surrounding liquid are clearly visible in the trace of Fig.4.3. The sharp increase at zero time delay (the time when pump and probe pulses are overlapped in time) stems from the excited hot electrons in the metal, which shift and broaden the surface plasmon resonance of the gold nanoparticle. Coupling between hot electrons and lattice phonons follows, and the two subsystems reach equilibrium in about 2 ps. A subsequent damped oscillation is observed from tens to about one hundred picoseconds because of the excitation of the acoustic breathing mode which periodically shifts the SPR and modulates the transmission at the probe wavelength. The slow decay at longer time scales arises from the cooling of the gold particle due to heat exchange with the surrounding water. The vibration frequency of the breathing mode (0, 0) is about 60 GHz, as shown in the Fourier transform spectrum in the insert of Fig.4.3. It corresponds to an oscillation time of about 16.7 ps. This measured frequency corresponds to the breathing mode of a gold sphere of 54 nm diameter [48].

We fit the oscillatory part in the trace with the following phenomenological equation [95]:

$$\Delta T(t) = A_1 Exp(-\frac{t}{\tau_1}) + A_2 Exp(-\frac{t}{\tau_2}) cos(\frac{2\pi t}{T_{br}} + \varphi), \tag{4.7}$$

where the exponential term reflects the optical contrast of particle cooling and the accompanying heating of the surrounding liquid, and τ_1 is the characteristic time of this exponential decay. The damped cosine term reflects the damped oscillation of the breathing mode. The quantities τ_2, T_{br}, φ are the characteristic decay time, vibrational period and phase of the damped oscillation. The constants A_1 and A_2 are the proportionality constants. Cooling of the particle is controlled by both interfacial thermal resistance between particle and matrix and heat diffusion in the surrounding medium [103]. The interfacial thermal resistance will dominate at short times, and the particle temperature change will decay exponentially [99, 104]. At longer time scales, heat diffusion in the surrounding medium will dominate the cooling [105], and the temperature of the particle should decrease as $t^{-3/2}$ at very long times [106], which is in qualitative agreement with the experimental results in ref.[105]. In the regime governed by the interfacial resistance, the cooling time is proportional to the particle radius [99]. We see a deviation from the exponential fit at long time delays in Fig.4.3, but we nevertheless fit the oscillation part with Eq.4.7 in the following, for simplicity.

We performed pump-probe measurements on single nanoparticles with variable CW heating powers from zero to a power very close to, but lower than the boiling threshold of water. We then extract the parameters of the decay by fit-

ting the damped oscillatory part in a trace with Eq.4.7. The results of two particles are shown in Fig.4.4. As we can see from Fig.4.4 (a, d), for both particles, the

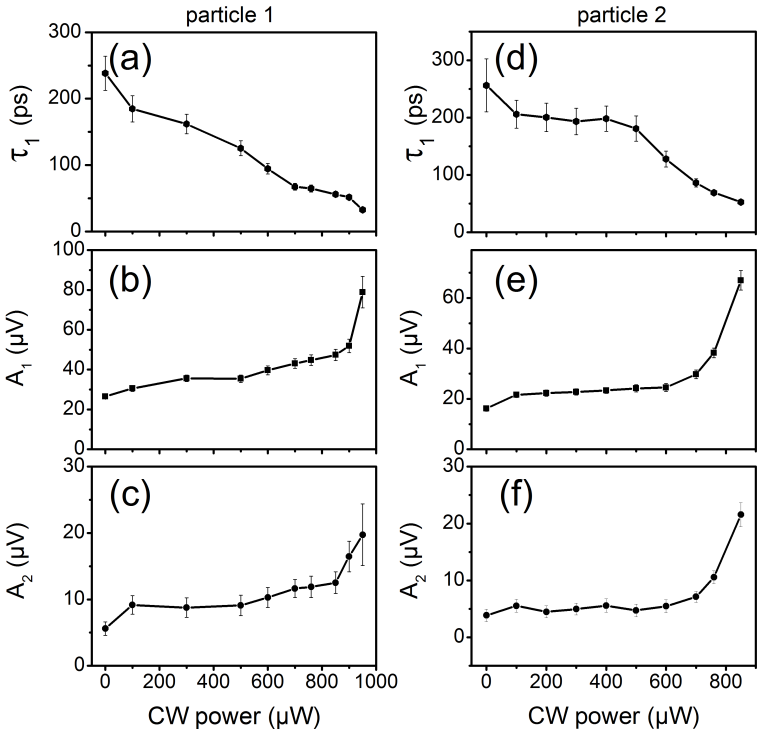

Figure 4.4: Parameters extracted from the fitting of the oscillatory part in the traces under variable CW heating powers. (a, b, c) show the changes of the characteristic decay time τ_1, and of the proportionality coefficients A_1 and A_2 as functions of the CW heating power. Measurements (a,b,c) were done on one particle and (d, e, f) on a second particle. For each particle, the pump and probe fluences remained the same in all measurements. The error bars in the plots represent the fitting uncertainty.

characteristic decay time τ_1 decreases steeply with the increase of CW heating powers. We do not think that this could result from any change of the interfacial thermal resistance at high heating power. The interfacial thermal resistance is related to the acoustic impedance mismatch of two contacting materials: Z_2/Z_1 [103], where $Z = \rho v$ is the acoustic impedance, ρ the density, v is the sound velocity of each material. The acoustic impedance of gold is almost independent of temperature below its melting point, while the acoustic impedance of water only decreases with temperature (both the sound velocity and the density decrease at high temperature). Therefore, we attribute this change in the characteristic decay time (τ_1) to the complexity of the optical signal in the strongly

inhomogeneous medium.

At heating powers less than 800 (600) μW for particle 1 (2), we can see a linear change in the proportionality coefficient A_1 which reflects the continuous heating of nearby liquid around the particle. Above a given threshold around 900 μW for particle 1 and 700 μW for particle 2, the proportionality coefficient A_1 increases suddenly to a much higher value. A similar sudden increase in slope was observed in our photothermal study of vapor nanobubbles [30], and we attributed it to the boiling of the nearby liquid and the formation of a vapor bubble. The estimated temperature of the gold particle from the threshold heating power is also close to the expected boiling temperature of water into a vapor nanobubble, calculated from the simple thermodynamic model (see Chapter 2 and Appendix C). We notice that the optical contrast of the acoustic vibration A_2 also becomes much higher above this threshold. Because we expect the vibration amplitude not to depend too strongly on the density of the medium surrounding the particle (the gold is much heavier than water and water steam), we attribute the change of A_2 to a plasmonic effect. When the bubble forms around the particle, there is a large refractive index change surrounding the particle. This will shift the SPR of the particle and largely change the extinction at probe wavelength. The changes in the extinction are more pronounced when the probe wavelength is on the red wing of the SPR peak, which is the case in our current measurements. Other fitted parameters such as τ_2, T_{br} and φ do not show much dependence on the CW heating power.

4.4.2. Time-resolved trace of vapor bubbles at high heating power

The kinetics of the optical signal upon cooling of the gold nanoparticle strongly suggests that at a high heating power close to the boiling threshold, a vapor bubble forms around the particle under the trigger pulses. Now we will look at the pump-probe traces in this regime of the vapor bubble.

In Fig.4.5, we plot the time-resolved traces of vapor bubbles from -10 ps to 900 ps time delays, as shown by the red curves. The two red traces are recorded with two different gold nanoparticles. The black curves in both plots are the pump-probe trace without CW heating, and are shown for comparison. We confirm the formation of vapor nanobubbles based on the following facts: first, we record traces at different CW heating powers, and we only observe such reproducible bubble traces when the heating power is high enough (see control experiments as the black curves). Second, the temperature rise of the gold particle calculated from the measured powers is close to the expected boiling temperature of water in nanobubble conditions (see details in Chapter 2 and Appendix C). Third, the contrast of the acoustic vibration of the particle be-

comes much stronger. Moreover, the damping decreases, leading to longer decay times, which is expected when the viscous damping of liquid water is removed (compare oscillations in the red and black curves). This could indicate an enhancement of the optical signal (the optical contrast of the acoustic vibration) by the index jump at particle-liquid interface caused by the bubble formation. The appearance of a vapor bubble enhances the extinction (SPR) changes of the gold particle at the probe wavelength. In a way, the bubble acts as an acousto-optical or acousto-plasmonic transducer for particle vibrations. Previous experiments with pump-probe spectroscopy on ensembles of gold nanoparticles in water found related results [107]. Signal enhancement at longer time delays was assigned to vapor bubble formation. The pump fluence found in these experiments also matched the threshold of explosive boiling of surrounding water [107].

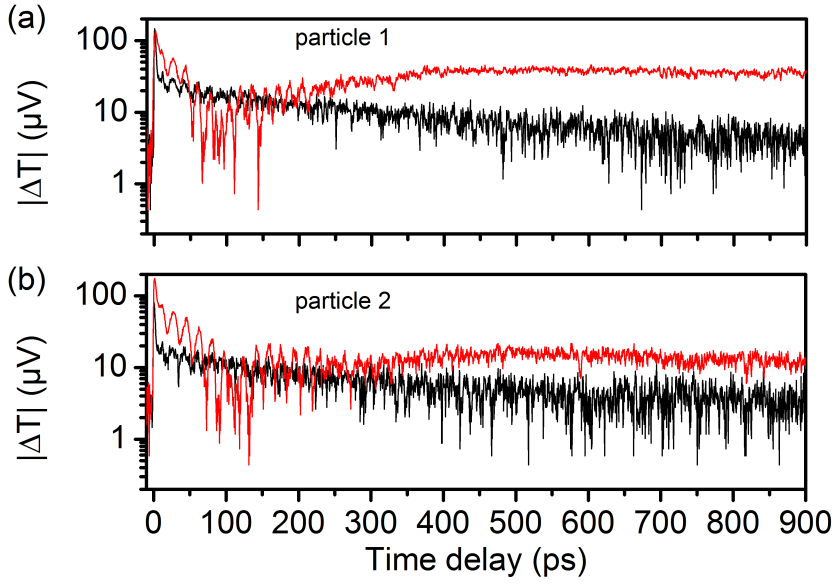

Figure 4.5: Two examples of transient traces of vapor nanobubbles measured by pump-probe spectroscopy for two particles in (a) and (b). The red traces with pronounced oscillations are obtained in the high heating power regime, when the bubble is thought to form (heating power 950 μW in (a), 850 μW in (b)). The black curves with more regular decays are the traces without CW heating for comparison. Note the more complex decay and the enhanced contrast of the breathing oscillations in the bubble traces. In all measurements, the pump and probe fluences remained the same (about 26 pJ per pulse at 785 nm and about 0.4 pJ per pulse at 597 nm). The integration time at each pixel is 30 ms.

We noticed that there is a characteristic interference feature in the bubble traces of Fig.4.5. The optical signal and extinction change sign at around 100 ps

after the pump triggering (zero time delay). Note that in the current measurements, we only record the absolute value (or the modulus) of the changes in the probe intensity which is the amplitude of the lock-in output. We attribute this interference feature to the bubble-size dependence of the total extinction of vapor bubble and gold nanoparticle. We calculated the extinction cross section of a vapor nanobubble around a 50 nm gold sphere at probe wavelength as a function of the vapor thickness using Mie theory, and we found that the extinction cross section first decreases steeply with the bubble thickness, reaches a minimum, and then increases when the bubble becomes much bigger. This can be understood by the fact that when the bubble grows and remains relatively small, the negative relative polarizability of the thin vapor shell will cancel out the positive relative polarizability of the gold nanoparticle. The whole system becomes less polarizable, and the total polarizability will decrease with bubble size. As the bubble grows further and overcomes a certain size where the extinction is minimal, the size of the vapor bubble becomes so large that it will optically "screen" the particle and dominate the extinction. The critical size or bubble thickness is found to be comparable to the size of particle radius. We tried to fit our data with the calculated extinction cross section, assuming the size of the vapor bubble goes linearly with time. We found the fitting can "reproduce" the interference feature very well. So the interference feature observed in the traces results from the dependence of the total extinction on the bubble size.

We also observed that the extinction signal when a vapor bubble forms around the gold particle is not very high, even though it is clearly different from the extinction at low heating powers. This suggests that the bubble is not very extended in size compared to the particle, at least during the first nanosecond. In principle, if a large vapor bubble forms around the gold particle, we expect a large SPR shift and a large scattering/extinction change at the probe wavelength. An alternative explanation for the relative weakness of the transmission change would be that not all pump pulses lead to bubbles, or that a jitter due to nucleation [3] broadens and weakens the transmission change. Pump-probe spectroscopy is based on stroboscopic measurements, which require good synchronization between a trigger pulse and the transient phenomenon under study. However, if the bubble is triggered acoustically by the particle's vibrations, the jitter should be negligible. Indeed, the jitter in our measurements seems not to be significant, as the extinction in Fig.4.5 goes all the way down to the minimum close to zero in both bubble traces of particle 1 and 2. Otherwise the extinction will become flattened if the jitter is large.

At this stage, we do not completely understand the dynamics of the vapor nanobubbles we observe in our experiments, and there are a number of open

questions, which require more detailed studies in the near future. For example, what is the size of the vapor bubble? How to explain the signal changes around 300 ps in Fig.4.5 (b), which is not present in Fig.4.5 (a)? Does the vapor bubble continue to grow or collapse at a certain point? A theoretical modeling of thermodynamics of vapor bubbles considering both pulsed and continuous heating will help understand the temporal profile of vapor bubble, while relating the extinction data measured in experiments with the thermodynamic modeling through Mie theory [108] can provide information such as bubble size, temperature and pressure. However, because this problem requires complex near-field optical simulations and modeling of ultrafast dynamics of soft matter at a phase transition, the calculations required were too complex to be performed within the limited time span of this work.

4.5. Conclusions

Combining pump-probe spectroscopy and continuous heating, we studied vapor bubbles in water around a 50 nm gold sphere with picosecond time resolution for one nanosecond. We found that the acoustic vibration of a gold nanoparticle becomes less damped when a vapor bubble forms around the gold particle. The enhancement of the optical contrast of vibration-induced oscillations confirms that vapor bubbles can indeed enhance acousto-optical transduction. In this chapter, we presented preliminary results and a qualitative discussion. A more detailed theoretical modeling of the bubble's dynamics would shed light on the understanding of our data and of vapor bubble properties.